Electronic Structure, Photophysics, and Relaxation Dynamics of Charge Transfer Excited States in Boron−Nitrogen-Bridged Ferrocene-Donor Organic-Acceptor Compounds

M. D. Thomson, M. Novosel, and H. G. Roskos*

Physikalisches Institut, Robert-Mayer-Strasse 2-4, Johann Wolfgang Goethe-Universität, D-60054 Frankfurt am Main, Germany

T. Müller, M. Scheibitz, and M. Wagner

Institut für Anorganische Chemie, Marie-Curie-Strasse 11, Johann Wolfgang Goethe-Universität, D-60439 Frankfurt am Main, Germany

F. Fabrizi de Biani and P. Zanello

Dipartimento di Chimica dell'Università, Via Aldo Moro, I-53100 Siena, Italy

Received: October 9, 2003; In Final Form: December 21, 2003

We present a study of the electronic, photophysical, and picosecond excited-state relaxation characteristics of a class of derivatives comprised of multiple bipyridylboronium acceptors covalently linked to a ferrocene donor. These compounds exhibit a broad visible absorption band, which we attribute to a metal-to-ligand charge transfer transition between the donor and the acceptor. A comparison of optical absorption, spectroelectrochemical, and theoretical results confirms the assignment of the band and provides information on the degree of electron delocalization between the donor and the acceptor. Picosecond transient absorption measurements reveal that the back-electron transfer relaxation is critically dependent on the structural flexibility of the bridging bonds between the donor and the acceptor. In the case where the acceptor substituents are free to rotate about the bridging bonds between the boron and the cyclopentadienyl rings of the ferrocene, a significant portion of the excited state decays directly back to the ground state on a time scale of ∼18 ps, whereas in the case where an additional *ansa*-bridge that connects acceptor substituents enforces a more rigid conformation, the ground-state recovery proceeds only on a ∼800-ps time scale. This demonstrates the importance of conformational degrees of freedom for the internal conversion and back-electron transfer in these systems.

Introduction

Optically induced charge transfer (CT) has a central role in many fundamental processes, such as those in biological systems,[1−3] as well as being a functional mechanism in various areas of optoelectronics, such as solar cells,[4,5] photoconductors[6,7] and nonlinear optical devices.[8] Of particular interest are materials that contain organometallic moieties, e.g., ferrocene (Fc), which possess desirable qualities because of their ability to exist in different stable oxidation and spin states,[9] and the ability to tune their properties by a suitable choice of substituents.[9−11] Several detailed studies exist on Fc-donor organic-acceptor metal-to-ligand charge transfer (MLCT) compounds in the context of nonlinear materials, where the donor and the acceptor are connected via conjugated bridges[8,12,13] and both the highest occupied molecular orbital (HOMO) and the lowest unoccupied molecular orbital (LUMO) are delocalized over the entire structure. Although these studies have covered a large number of various organic acceptors, as well as the use of other bridging units (e.g., −C═N−[14,15]), there is still much scope for the development of new materials. Moreover, only very few studies exist on the excited-state photophysics and relaxation of the MLCT states in Fc-donor organic-acceptor compounds,[16,17] despite the fact that many interesting excited-state phenomena have been observed in other organometallic CT compounds.[18−22]

In this paper, we present a study of novel organometallic CT compounds that are composed of a Fc donor and multiple organic (bipyridylboronium, B-bipy) acceptors, connected by bridging bonds between C atoms on the cyclopentadienyl (Cp) rings and the 4-coordinated B atom (see structures **1-X**, **2-X**, and **3**−**7** in Figure 1), which have previously been characterized by NMR, electrochemical, and crystal structure analysis.[23−25] The spontaneous formation of B−N bonds allows one to achieve sophisticated target structures less readily accessible using conventional organic methodologies. This approach has been successfully applied in the synthesis of *ansa*-metallocenes[26,27] and oligometallic complexes,[28,29] which are related to the prototype monomers presented here. Because these compounds can undergo reversible oxidation and multiple reduction steps, they potentially allow electronic switching of their (nonlinear) optical properties. We are interested in electronic interaction and optical excitation across the B−N bonds, especially in terms of their use as versatile linkers between electron donors and polymers that exhibit strong electronic and magnetic correlation phenomena.[30] The properties of B−N bonds when incorporated into molecular assemblies still are not fully understood, although the basic properties of B−N bonds have attracted several recent theoretical studies.[31−35]

* Author to whom correspondence should be addressed. E-mail address: roskos@physik.uni-frankfurt.de.

10.1021/jp037044p CCC: $27.50
Published on Web 03/19/2004

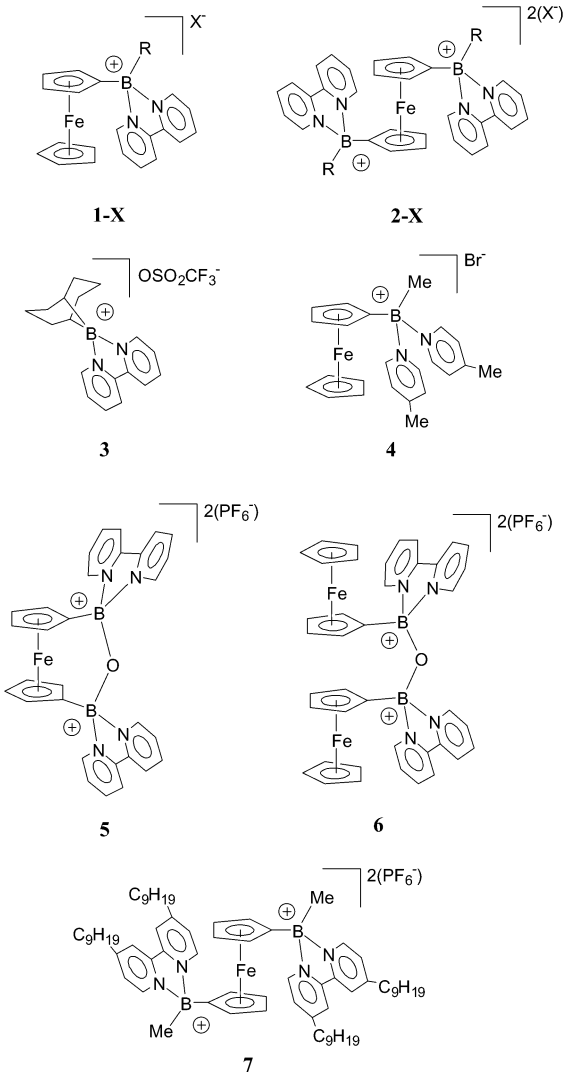

Figure 1. Ferrocene-donor bipyridylboronium-acceptor and control compounds under study here. (For compounds **1-X** and **2-X** the counteranion is $X^- = PF_6^-$, or Br^-. Note that, unless otherwise specified, $R = CH_3$ in the text.)

Here, we combine UV−Vis, spectroelectrochemical, and picosecond transient absorption measurements with theoretical calculations, which confirm that the observed visible optical transition corresponds to a through-bond MLCT transition between the Fc and B-bipy units. Comparison of the derivatives **2-PF$_6$**, **5**, and **6** allows us to determine how the MLCT transition and excited-state evolution are affected by certain structural and electronic factors. For the compounds **1-PF$_6$** and **2-PF$_6$**, NMR measurements[23] indicate that the uncoupled acceptor groups are free to rotate about the B−C(Cp) bridging bonds. In the case of compounds **5** and **6**, the CH_3 groups at the B-sites have been replaced by an O atom that forms a bridge between the B atoms of each B-bipy acceptor group, such that the electronic environment is relatively similar between the two compounds, as evidenced by cyclovoltammetry measurements.[25] However, NMR measurements[24,25] reveal that the rotational freedom of the B−C(Cp) bonds in the *ansa*-form (**5**) is suppressed, whereas for the diferrocene compound (**6**), this degree of freedom is still retained. Electrochemical measurements for both derivatives **5** and **6**[24,25] suggest a moderate amount of electronic communication between the B-bipy groups across this bridge, so that these compounds allow the study of the effect of electronic coupling between acceptors on the CT states. A comparison of the two

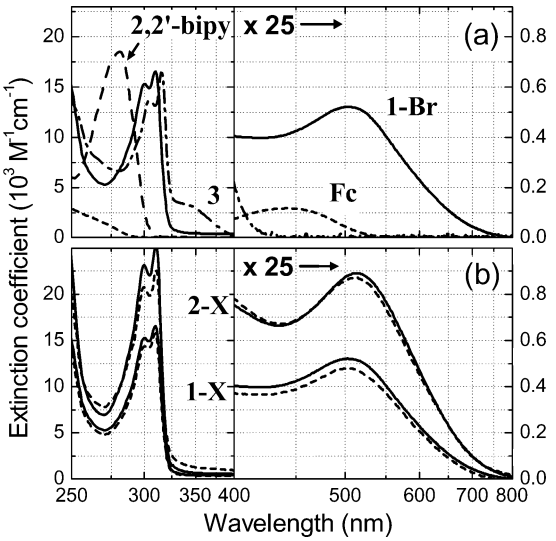

Figure 2. (a) UV−Vis absorption spectra of (—) **1-Br** and isolated fragment compounds, (- - -) ferrocene, (— — —) 2,2′-bipyridine, and (— • —) **3** (in CH_3CN). (b) Comparison of ***n*-X** versus the number of acceptor substituents ($n = 1.2$ as indicated) and counteranions **X = Br** (solid) and **X = PF$_6^-$** (dashed).

compounds allows us to isolate the effect of structural rigidity of the bridging bonds between the donor and acceptor groups.

From the picosecond transient absorption measurements of the back-electron transfer (bET) dynamics for the derivatives **2-PF$_6$**, **5**, and **6**, we find that the structural flexibility of the bridging bonds between the donor and the acceptor strongly affects the rate and mechanism for the bET. Specifically, in the case of compound **2-PF$_6$**, a significant fraction (∼45%) of the excited ensemble relaxes directly back to the ground state with a time constant of 18 ps, whereas for compound **5**, the ground-state recovery occurs only on a much slower time scale (∼800 ps).

UV−Vis Absorption Spectra

Figure 2a shows the UV−Vis absorption spectra of **1-Br** and of ferrocene, 2,2′-bipyridine, and compound **3** (all in CH_3CN), for comparison. For **1-Br**, two dominant absorption bands can be resolved: one is centered at 310 nm, and a broad visible absorption band with a peak near 500 nm is observed. Comparison with the spectra of 2,2′-bipyridine and **3** shows that this UV band at 310 nm corresponds to a modified $\pi-\pi^*$ transition between states localized on the B-bipy substituent, with the absorption peak of **1-Br** and **3** red-shifted some 35 nm (2900 cm^{-1}), relative to 2,2′-bipyridine, because of the modification of the π and π^* energy levels resulting from the increased electronegativity of the boron-coordinated N atoms.

The origin of the broad visible band is attributed to an intramolecular MLCT transition from orbitals concentrated on the Fc donor into those of the B-bipy acceptor, based on the following observations. As shown in Figure 2b, the character of the visible band is almost independent of the counteranion, and the absorption strength increases in proportion with the number of acceptor substituents (also confirmed for the case of four acceptor substituents, $\lambda_{max} = 540$ nm, $\epsilon_{max} = 1700$ M^{-1} cm^{-1}; see ref 23). Although this would be consistent with a transition localized on isolated B-bipy chromophores, this is ruled out by the absence of any absorptive feature in the Vis region in the spectra of compound **3**. Moreover, previous synthetic studies[23] have shown that the visible transition is absent in compound **4**, where the C−C bond between the two pyridine

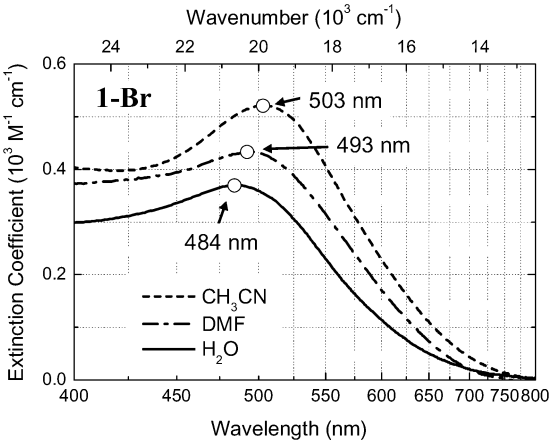

Figure 3. MLCT absorption band for **1-Br** in various polar solvents ((- - -) CH_3CN, (− · −) dimethylformamide (DMF), (—) H_2O) demonstrating negative solvatochromism and decreasing absorption strength with solvent polarizability.

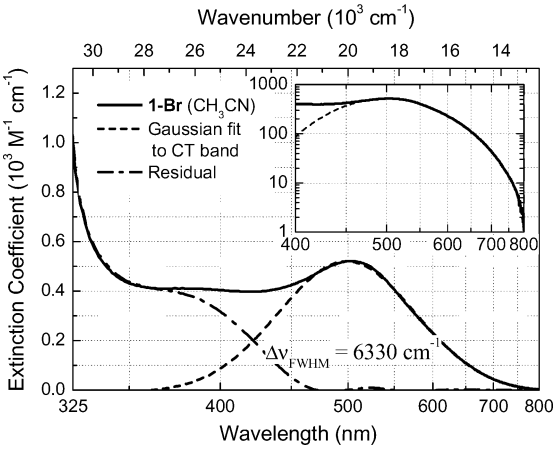

Figure 4. (- - -) Gaussian fit to MLCT band for (—) **1-Br** (in CH_3CN) and (− · −) residual absorption. Inset uses a logarithmic vertical scale.

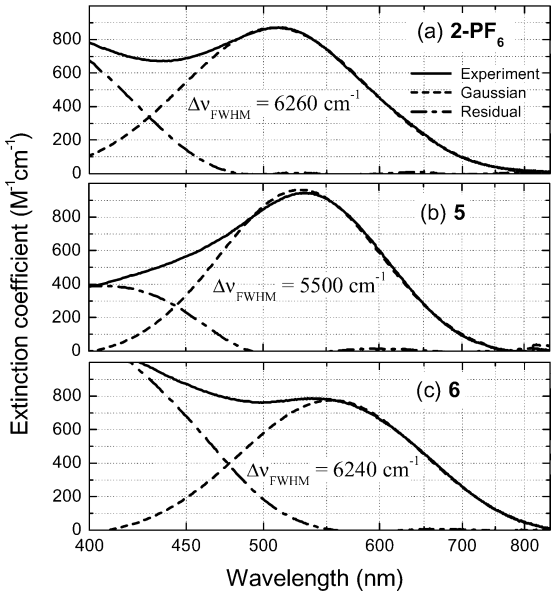

Figure 5. MLCT absorption spectra (solid lines) of (a) **2-PF$_6$**, and the B−O−B bridged-acceptor compounds (b) **5** and (c) **6** (all in CH_3CN) relevant to the electrochemistry and transient absorption measurements. Also shown are the single Gaussian curves fitted to (- - -) the low-energy side of the absorption band and (− · −) the residual absorption.

rings has been removed (which has the effect of strongly degrading the electron-accepting quality of the substituent without posing any significant changes in the structural or electronic environment seen by electronic states localized on the Fc unit). This rules out the possibility that the transition only involves orbitals that are localized on the Fc unit.

Figure 3 shows the effect of solvent interaction on the absorption spectra for **1-Br**, which shows a marked negative solvatochromism in going from CH_3CN to H_2O ($\Delta\nu = 780$ cm^{-1} for **1-Br** and $\Delta\nu = 710$ cm^{-1} for **2-Br**). This behavior has been observed for CT transitions in similar cationic species,[8,13] contrary to the typical positive solvatochromism of CT transitions in neutral species, and is to be expected, based on the fact that the ground state in these cationic species is actually more polar (and, hence, more strongly stabilized by polar solvents) than the CT excited state. Moreover, the strength of the transition decreases as the solvent polarizability increases, which suggests that the solvent interaction causes a Stokes shift between the ground state and the excited state, which affects the Franck−Condon factor for the transition. Given these observations, we also attribute the small red-shift of the absorption band of compound **2-X**, relative to compound **1-X** ($\Delta\nu = -349$ cm^{-1} for **X** = **PF$_6$**$^-$), in Figure 2 to a reduced stabilization of the ground state in compound **2-X**, because of the reduction in polarity, which results from the symmetric positions of the two acceptor groups.

To better resolve the MLCT band from the absorptive shoulder on the blue side, we fit the low-energy portion of the band with a single Gaussian function, $\epsilon(\nu)$,[36] which, as shown in Figure 4, reproduces the resolvable portion of the band exceptionally well, yielding a full width (at half-maximum) of $\Delta\nu_{fwhm} = 6330$ cm^{-1}, and an estimate for the oscillator strength of $f \approx 0.014$.[37] Subtracting this fitted Gaussian from the total absorption spectrum yields a physically acceptable residual absorption profile (see Figure 4), which shows evidence for another absorption band with an absorption maximum near 380 nm that is partially resolvable from the onset of the 310-nm B-bipy UV absorption band. The fact that the low-energy portion of the MLCT band fits very closely to a single Gaussian function suggests that only a single electronic transition is involved, although the question arises as to the origin of the strong line broadening (see below).

Figure 5 displays the absorption spectra for compounds **2-PF$_6$**, **5**, and **6** (in CH_3CN), which all exhibit a similar MLCT band. As can be seen, the visible absorption band peaks of both compound **5** ($\lambda_{max} = 532$ nm) and compound **6** ($\lambda_{max} = 554$ nm) are red-shifted, relative to compound **2-PF$_6$** ($\Delta\nu = -785$ cm^{-1} and $\Delta\nu = -990$ cm^{-1}, respectively), which is indicative of an increasing stabilization of the acceptor LUMO in these compounds, because of the aforementioned electronic communication between acceptors across the −O− bridge. We note that the absorption band of a derivative of **1-PF$_6$** with R = −OH is significantly less red-shifted ($\lambda_{max} = 523$ nm), which rules out the possibility that the effect is purely due to the electron-withdrawing effects of the O atom. For compounds **2-PF$_6$** and **6**, the lower-energy side of the MLCT band is still very closely Gaussian, with fitted fwhm widths very similar to that of **1-Br** ($\Delta\nu_{fwhm} = 6260$ and 6240 cm^{-1} for compounds **2-PF$_6$** and **6**, respectively), whereas for the case of compound **5**, the fwhm is reduced by ∼10%−15% ($\Delta\nu_{fwhm} = 5500$ cm^{-1}) and slight deviations from a Gaussian form are evident.

Three main mechanisms could be responsible for the broad, featureless MLCT band, which we discuss, in turn, in the following.

(1) Given the significant rearrangement of the electronic charge distribution upon excitation, a strong interaction between

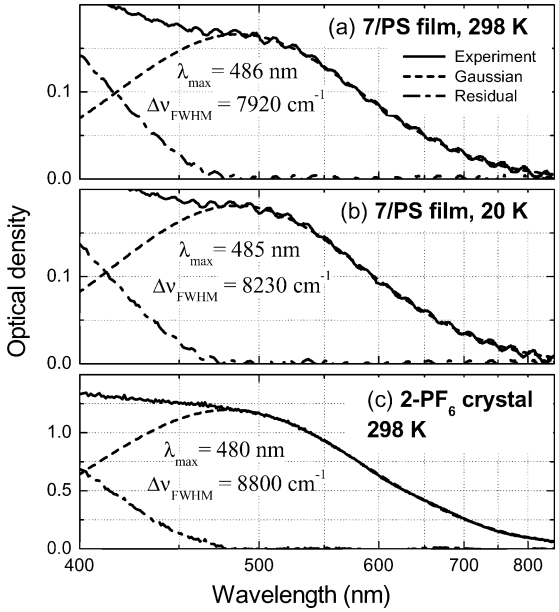

Figure 6. MLCT absorption band and Gaussian fits for compound **7** in a drop-cast polystyrene film (~10 μm thick) at (a) 298 K and (b) 20 K (note that the modulation of the curves is due to multiple pass interference). (c) Corresponding absorption for the compound **2-PF$_6$** crystal sample.

the solute and the distribution of local polar solvent molecules can lead to considerable line width broadening. To remove the role of polar solvation on the MLCT transition, we have also performed measurements on thin polystyrene films that have been doped with compound **7** (a close derivative of compound **2-PF$_6$**, only with additional nonyl chains attached to the pyridine rings for improved solubility), which were drop-cast from a tetrahydrofuran (THF) solution. The measured MLCT absorption spectra are shown in Figure 6, both at room temperature (see Figure 6a) and at 20 K (see Figure 6b). The MLCT absorption band at 298 K is similar to that in solution, although somewhat blue-shifted (λ_{max} = 486 nm) and additionally broadened ($\Delta\nu_{fwhm}$ = 7920 cm^{-1}). Considering such modest changes upon switching to the relatively nonpolar polymer environment, one can rule out solvation as the key source of broadening. We also note that cooling the film to 20 K leads to only very small changes in the absorption spectrum (with the width of the spectrum actually increasing ~4%) and does not reveal any resolvable structure. This suggests that the width of the spectrum is not associated with a thermal distribution of ground-state vibrational levels (at least for vibrational quanta >14 cm^{-1}).

(2) In analogy to *intermolecular* CT between separate donor and acceptor molecules, a distribution of relative distances and/or orientations between the donor and the acceptor can result in appreciable broadening in the transition energy.[38,39] This could be applicable for compounds **1-X**, **2-X**, and **6**, where the unhindered rotation about the B−C(Cp) bonds yields such a conformational distribution. However, this degree of freedom is strongly hindered for compound **5** and, hence, is unlikely to account for the majority of broadening observed. To examine this further, we have also performed absorption measurements on a thin crystalline sample of **2-PF$_6$** (Figure 6c), where all molecules share the same fixed conformation. As can be seen, the MLCT band is even further blue-shifted and broadened (λ_{max} = 480 nm, $\Delta\nu_{fwhm}$ = 8800 cm^{-1}), ruling out the role of a conformational distribution. Hence, we attribute the majority of the line width to the final mechanism.

(3) A large displacement in the equilibria of certain modes between the ground and excited states results in a broad manifold of closely spaced vibrational transitions with a Gaussian envelope. Presumably, any residual structure is washed out by additional broadening, because of rapid dephasing of the initial excited state.[40]

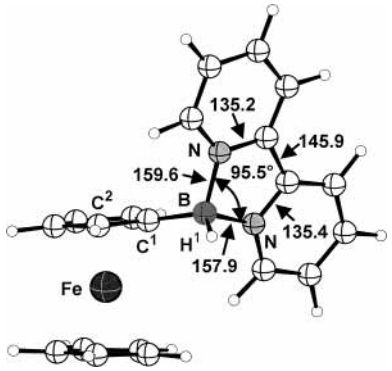

Figure 7. Calculated gas-phase structure of compound **1** (with R = H) (using B3P86/6-31G(d) for C, B, N, H and SDD for Fe). All bond lengths reported in picometers.

Returning to Figure 5, we also note that, for compounds **2-X**, **5**, and **6**, the relative orientation (or distribution thereof) and, hence, through-space separation of the acceptor groups, relative to the Fe core, vary significantly, whereas the through-bond distances are relatively constant.[23−25] The absorption character and strength are comparable for these compounds, which leads us to conclude that the MLCT is due to through-bond coupling between the donor and acceptor orbitals across the (Cp)C−B−N network, as opposed to through-space.

In terms of the relaxation of the MLCT excited states, we note that no measurable luminescence in the range of 500−900 nm (i.e., a quantum efficiency of <0.05%) or photochemistry was observed upon excitation of the MLCT band for all the derivatives tested, which suggests that the relaxation occurs through nonradiative photophysical pathways, which are addressed in the section that presents the picosecond transient absorption results.

Quantum Chemistry Calculations and Electronic Structure

Gas-phase calculations were performed on the monocation **1** (with R = H), to substantiate and better understand the origin of the MLCT transition between the donor and the acceptor. Geometry optimizations were performed at the hybrid density functional level of theory, using Becke's three-parameter functional with the nonlocal correlation provided by the Perdew-86 equation (B3P86) in connection with the 6-31G(d) basis set for carbon, boron, nitrogen, and hydrogen.[41] For iron, the SDD pseudopotential was used, in combination with a DZP valence basis set.[42−44] This model has provided theoretical structures for ferrocene that are very close to those experimentally determined from gas-phase measurements.[45] The UV−Vis transition energies were calculated with the time-dependent (TD) method,[46] using a 6-31+G(d) basis set.

These density functional calculations predict a theoretical structure (see Figure 7) that is very close to the experimentally determined crystal structure for compound **1-PF$_6$**.[23] Even very weak modes (for example, the conformation of the B−R bond, relative to the plane of the C_5H_5 ring of the ferrocenyl group) are reproduced by our computational model (i.e., $\Theta(H^1BC^1C^2)$ = 35° (theory), compared to $\Theta(MeBC^1C^2)$ = 39.7° (experiment)[23]). This correspondence implies that certain distortions of the structure of **1-PF$_6$** reported in ref 23 result because of internal molecular forces, as opposed to crystal packing forces.

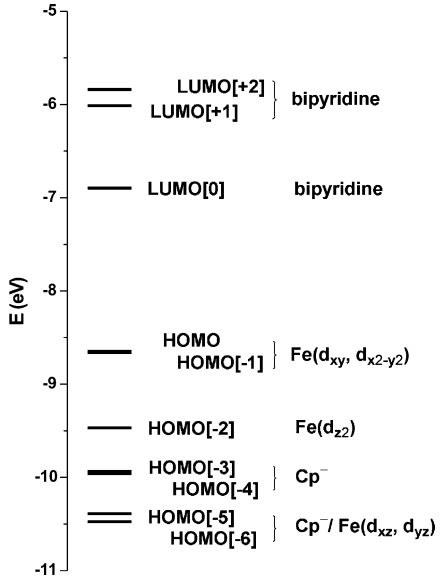

Figure 8. Calculated energy diagram for the frontier orbitals of compound **1** (R = H).

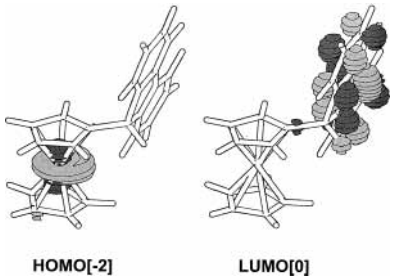

Figure 9. Qualitative molecular orbital diagram for selected frontier orbitals consistent with MLCT transitions.

TABLE 1: Low-Energy Optical Transitions for 1 (R=H) and Corresponding Dominant Molecular Orbitals Predicted by the Time-Dependent Density Functional Theory (TD−DFT) Calculations

HOMO[*m*]	LUMO[*n*]	E_{max} (eV)	λ_{max} (nm)	oscillator strength, *f*
0	0	1.17	1058	0.0006
−1	0	1.21	1029	0.0028
−2	0	2.01	618	0.0084
0	+1	2.08	598	0.0004
−1	+1	2.11	589	0.0030
0	+2	2.26	548	0.0013
−1	+2	2.28	544	0.0004
−3/−4	0	2.49	499	0.0013
−3/−4	0	2.52	492	0.0003

An energy diagram of the calculated frontier orbitals (calculated at the B3P86/6-31+G(d) level) are shown in Figure 8, with selected orbitals being shown in Figure 9. The frontier orbitals can be divided into three groups: (i) relatively low-lying molecular orbitals with main contributions from the cyclopentadienyl substituent (HOMO[−3] and HOMO[−4]); (ii) metal-centered orbitals, essentially of nonbonding character, which are the highest occupied orbitals (HOMO[−2]−HOMO[0]); and (iii) vacant orbitals of low energy (LUMO[0]−LUMO[+2]) that are centered on the bipyridine unit.

Transition energies and oscillator strengths from the TD calculation are presented in Table 1. These results provide evidence that the lowest-energy optical transitions result from excitations from Fc-based occupied orbitals into unoccupied orbitals located on the bipyridine unit. The predicted oscillator strengths are relatively small, most probably because of a small spatial overlap between the donor and acceptor orbitals. The most intense absorption, according to the calculations, results from excitations from the HOMO[−2], predominantly of Fe(d_{z^2}) character, into the LUMO[0]. This transition has a predicted oscillator strength of $f = 0.0084$ (which is of the same order of magnitude as the estimate of 0.014 that is extracted from the experimental absorption spectra). Moreover, the fact that the transition energy predicted from the gas-phase calculation ($\lambda_{max} = 618$ nm) is lower than the measured value in solution is consistent with the negative solvatochromism reported in the last section.

In addition to the model calculations for the monocation **1** (R = H) discussed here, we also performed the corresponding ground-state calculation for the dication (i.e., the same single-acceptor compound with one electron removed), to gain a better understanding of the electronic changes to be expected upon electrochemical oxidation of an electron from the Fc-centered HOMO (discussed in the following sections). These results confirm that electron removal strongly increases the binding energy of all molecular orbitals, with the frontier (Fc-centered) occupied molecular orbitals being more strongly stabilized than the B-Bipy-centered unoccupied MOs. This leads to an increase in the energy between the HOMO[−2] and LUMO[0] from 2.6 eV for the monocation to 4.9 eV for the dication. Assuming that the error due to approximating the optical transition energies by HOMO/LUMO energy spacings is the same for the two redox states, this increase in energy suggests that the MLCT band would be blue-shifted some 2.3 eV, which corresponds to a peak wavelength of <300 nm (based on the experimental peak value for **1-Br** in solution of ∼500 nm).

Electrochemistry

Electrochemical measurements allow one to extract useful correlations between the oxidized-donor and reduced-acceptor species (D^+A and DA^-) and those of a weakly coupled CT excited state, which can often be well-represented as an excited redox pair, $(D^+A^-)^*$.[47,48] By examining trends in the redox potentials versus the energy of the CT transitions for a set of related compounds, one can estimate the degree of interaction between the relevant donor and acceptor molecular orbitals and reorganization energy upon CT,[49] whereas UV−Vis spectroelectrochemistry data can provide details on the effect of CT on the frontier orbitals and suggest expected spectroscopic properties of the excited MLCT state for comparison, e.g., with transient excited-state absorption measurements.[20] Generally, the range of compounds under study here readily undergo reversible oxidation and reduction steps, allowing a relatively straightforward interpretation of the redox measurements. From these measurements, one can also gain insight into how the linear and nonlinear optical properties of the system (governed by the MLCT) may be reversibly switched by external electronic means.[50,51]

Figure 10a and b present typical cyclovoltammetry traces of compounds **2-PF$_6$** and **5**, respectively (reported previously[23,24] but reprinted here for comparison). In both compounds, a single one-electron (1-e$^-$) oxidation peak is present, at $E_{ox}^{o\prime} = +0.43$ V (**2-PF$_6$**) and +0.57 V (**5**) (denoted by "ox" in both graphs), which is derived from the removal of an electron centered on the Fc unit (note that $E_{ox}^{o\prime} = +0.49$ V for ferrocene under the same conditions), and testifies that the presence of the acceptor groups attached to the Cp rings leads to only a small perturbation of the donor orbitals relevant to oxidation. At a negative cell potential, compound **2-PF$_6$** exhibits two reduction waves (denoted "red,1" and "red,2"), each of which has been shown

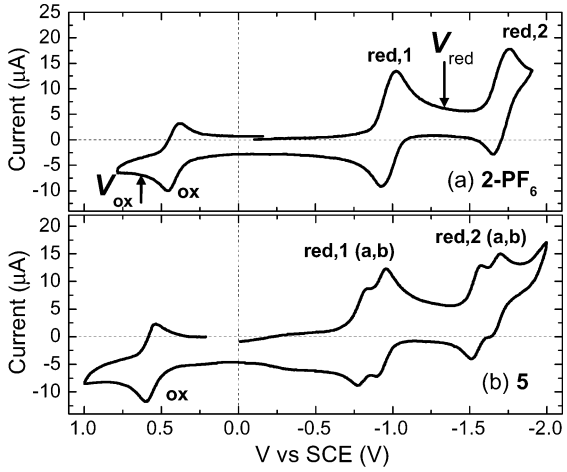

Figure 10. Cyclic voltammograms of (a) compound **2-PF$_6$** and (b) compound **5** indicating the 1-e$^-$ oxidation (ox) and first (red,1) and second (red,2) 2-e$^-$ reduction waves (both with 0.6×10^{-3} mol dm^{-3} in DMF containing 0.2 mol dm^{-3} [NEt_4][PF_6], platinum electrode, scan rate of 0.2 mol dm^{-3}). "V_{ox}" and "V_{red}" denote the static potentials used for the UV−Vis spectroelectrochemical measurements.

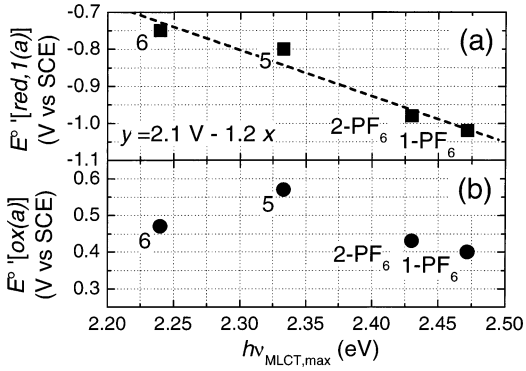

Figure 11. Graph of (a) first reduction-wave potential $E^{\circ\prime}_{red,1(a)}$ and (b) oxidation-wave potential $E^{\circ\prime}_{ox(a)}$ for compounds **1-PF$_6$**, **2-PF$_6$**, **5**, and **6** versus MLCT absorption peak energy (in CH_3CN). (A linear fit to the reduction wave potentials is included in Figure 11a, as indicated.)

to involve the addition of two electrons (one electron per acceptor unit).[23] In comparison with the cyclovoltammetry trace of compound **1-PF$_6$** (which features two 1-e$^-$ reduction waves),[23] both reduction peaks are only slightly shifted and broadened, because of the presence of the second acceptor unit (i.e., $E^{\circ\prime}_{red,1} = -1.02$ V for **1-PF$_6$** and $E^{\circ\prime}_{red,1} = -0.98$ V for **2-PF$_6$**), which implies only a weak interaction between the acceptor groups in compound **2-PF$_6$**. In contrast, it is evident in Figure 10b that, for compound **5**, the degeneracy between the two electrons in each reduction step is lifted (e.g., for the first 2-e$^-$ reduction, $E^{\circ\prime}_{red,1a} = -0.80$ V, $E^{\circ\prime}_{red,1b} = -0.93$ V),[24] which indicates significant interaction between the acceptor units. As mentioned previously, this interaction is most likely due to a degree of through-bond communication across the −O− bridge, and the additional shift to less-negative potentials is consistent with the red-shift seen in the UV absorption band for this compound.

To test the correspondence between the energy levels of the redox pairs and the observed CT bands, we plot the relevant redox potential data against the corresponding UV−Vis absorption maxima of the MLCT bands in Figure 11 for compounds **1-PF$_6$**, **2-PF$_6$**, **5**, and **6**. Figure 11a shows that the reduction potential fits a linear trend fairly well (as shown); in this figure, the potential progresses to less-negative values (and, hence, the LUMO is increasingly stabilized) as the MLCT band transition

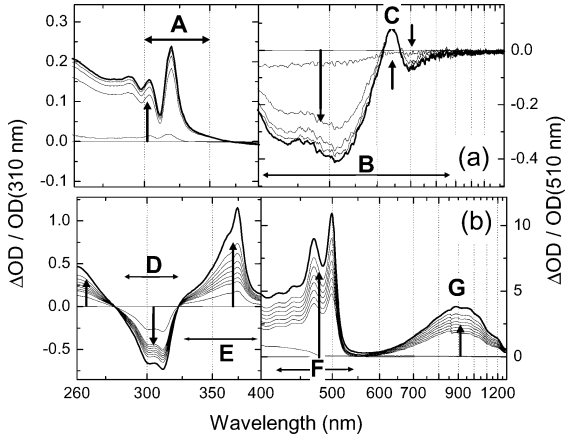

Figure 12. Time-series differential absorption spectra of compound **2-PF$_6$** (DMF) upon (a) 1-e$^-$ oxidation and (b) first 2-e$^-$ reduction (experimental conditions and static redox potentials (V_{ox}, V_{red}) as indicated in Figure 10). UV (left) and Vis (right) data are normalized to the initial absorption band peaks as indicated. (Note that all qualitative features were also reproduced in the corresponding measurements on **1-PF$_6$**.)

energy decreases, which is consistent with the hypothesis that both the first reduction and the MLCT transition involve LUMO[0]. In contrast, the oxidation potential (Figure 11b) shows only a weak correspondence with the MLCT transition energy. One possible explanation for this phenomenon refers to the predictions of the orbital calculations of the previous section, where the results suggest that the observed MLCT band results not from the HOMO[0] located on the ferrocene, but rather between the HOMO[−2] and the LUMO[0] on the acceptor. Assuming that the observed oxidation (reduction) processes involve the removal (addition) of an electron from (into) the primary frontier orbitals (HOMO[0] and LUMO[0]), one should only expect a direct correlation of the CT transition energy with the observed reduction potentials.

Figure 12 shows the change in UV−Vis absorption spectra for compound **2-PF$_6$** during exhaustive oxidation (Figure 12a) and 2-e$^-$ reduction (Figure 12b) (at the static potentials indicated in Figure 10). In Figure 12a (oxidation), the increase in absorption in the region of 300−350 nm (labeled band "A") corresponds to an increase in the strength and reshaping of the modified $\pi-\pi^*$ transition, which is associated with the B-bipy unit (see Figure 2), because of the increased electronegativity of the oxidized Fc unit. The broad feature in the range of 370−900 nm that exhibits a negative differential absorption is due to the suppression of the MLCT band, which reflects the strong energetic changes between the associated molecular orbitals upon oxidation, as mentioned at the end of the theoretical results section. However, several new absorptive features are manifested in this range (which is evident from the oscillatory structure in the region labeled "B"), including a band which results in a net absorption increase, which is observed from the small positive region of the curve ($\lambda_{max} = 637$ nm, labeled "C"). This spectral feature is in almost quantitative agreement with previous reports of the absorption changes upon oxidation of ferrocene to form the ferrocenium cation.[52] We assign this band to a transition from some low-energy Fc-centered occupied molecular orbital into the HOMO[0] orbital, which can accommodate one electron after oxidation.

The corresponding absorption changes upon reduction of compound **2-PF$_6$** (Figure 12b) are markedly larger in magnitude. In the UV range, one observes an almost-complete depletion of the original B-bipy absorption band (labeled "D"). Two new bands (labeled "E" and "F"), in the range of 320−500 nm,

appear: band E exhibits one clear maximum at 374 nm, whereas band F possesses a resolvable vibrational structure, with the first two lowest-energy peaks at 470 and 500 nm ($\Delta\nu = 1260$ cm^{-1}). These absorption bands have been reported[53] for reduced $[bipy\text{-}BR_2]^+$ compounds (with aromatic or alicyclic substituents attached to the 4-coordinated B atom); e.g., for compound **3-PF$_6$**, the corresponding peak positions are $\lambda_{max} = 378$ nm (band E) and 463/494 nm (band F). However, ref 53 reported that, in the case where electron-attracting O or F ligands are attached to the B atom, band F is significantly blue-shifted ($\lambda_{max} = 422/460$ nm), whereas band E is relatively unaffected by the nature of the ligands. We will return briefly to this point in the following section when interpreting the excited-state transient spectra. In the case of CT excitation (as opposed to sole reduction of the acceptor), one would expect the Fc to become more electron-withdrawing and, hence, produce such a blue-shift of band F. The last feature is a broad Vis−NIR absorption band (band "G"). This absorption band is unlikely to result from CT transitions from Fc onto the acceptor, which should generally be blue-shifted upon reduction of the acceptor. Hence, we attribute this new band to a transition localized on the reduced B-bipy units.

Several key results emerge from the electrochemistry data presented here. The linear relationship between the peak absorption energies and reduction potentials supports a MLCT transition between the weakly coupled donor and acceptor, whereas the poor correlation with the oxidation potentials is consistent with the theoretical prediction that the CT transition originates from lower-lying occupied molecular orbitals. Moreover, as will be shown in the next section, the UV−Vis absorption changes upon oxidation/reduction are in qualitative agreement with the transient spectra and aid in the interpretation of the excited-state dynamics.

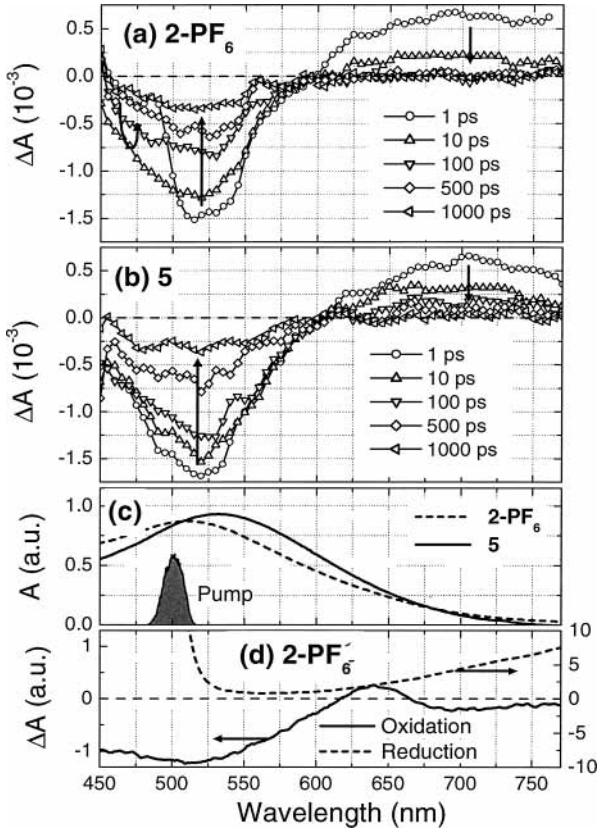

Figure 13. Picosecond transient absorption spectra of (a) compound **2-PF$_6$** and (b) compound **5** ($\lambda_{pump} = 500$ nm, ~3.5 mM in CH_3CN in both cases) at selected pump−probe delays. (c) Ground-state absorption and excitation spectra. (d) Differential spectra of compound **2-PF$_6$** upon electrochemical oxidation and reduction.

Transient Absorption Measurements

To understand the nonradiative relaxation dynamics of the MLCT state, we performed transient absorption measurements, using the femtosecond (fs) pump−probe technique. For the excitation (pump) pulses, we used 30-fs pulses that were tuned to a center wavelength of 500 nm from a commercially obtained noncollinear OPA (NOPA),[54] which is pumped by a 1-kHz Ti:sapphire amplifier laser that produces 150-fs pulses with a center wavelength of 775 nm (Clark-MXR CPA-2001). For the broadband probe source, we used white-light continuum pulses[55−57] that were generated by focusing a small fraction of the 775-nm light into a 3-mm-thick sapphire disk, producing a usable white-light spectrum from 450 nm to 770 nm. To minimize temporal dispersion, an off-axis paraboloidal mirror with an effective focal length of $f = 50$ mm was used to collimate the white-light probe beam. A second paraboloid ($f = 100$ mm) was used to focus the noncollinear pump and probe beams into the sample (a static 1-mm-thick cuvette, ~3.5 mM in CH_3CN). This yielded an instrument response of ~100 fs (as determined from control measurements with a rhodamine 6G sample, which was also used for determination of the zero-delay position versus probe wavelength). In all the kinetic data presented, the temporal region about a zero delay, which exhibits a relatively strong coherent artifact (due to nonlinear refraction that occurs in the cuvette and solvent[58]), has been removed. The pump−pulse energy used in these experiments was ~70 nJ. After the sample, the white-light probe was dispersed by a computer-controlled monochromator with a bandpass ~5 nm wide and was detected by a silicon photodetector. A custom-built mechanical chopper was used ahead of the sample to downsample the pump and probe pulse trains to 333 and 500 Hz, respectively, which allows the differential transient absorption signal to be detected by a lock-in amplifier at the 166-Hz difference frequency (which also rejected any uncontrolled stray pump light). Care was taken to ensure that the shape of the measured signals was not dependent on the pump and probe fluences, and that the white-light probe was focused more tightly in the sample than the pump beam, to avoid measurement errors that are due to the radial spatial chirp of the white light.

Figure 13 shows the transient absorption spectra for compounds **2-PF$_6$** (Figure 13a) and **5** (Figure 13b) (both in CH_3CN), following excitation at 500 nm, for a set of selected delays in the range of 1−1000 ps over the wavelength range of 450−770 nm, along with the relevant ground-state absorption and pump−pulse spectra in Figure 13c and the differential spectra that results from electrochemical oxidation and reduction (Figure 13d). Evident for both compounds is a negative-differential absorption band that extends from ~460 nm to 600 nm, where the saturation (bleach) of the MLCT absorption band dominates, whereas at wavelengths above a quasi-isosbestic point near 600 nm, a region of dominant excited-state absorption (ESA) is present, which extends at least to the red edge of the measurement window at 770 nm. Comparison with Figure 13c indicates that, although the bleach band is no longer dominant at wavelengths of >600 nm, the strength of the ground-state absorption band at this wavelength is still ~50% of that of the absorption maximum. Moreover, although the regions of bleach and ESA signals decay at clearly different rates for compound **2-PF$_6$** (discussed further below), the position of the zero-crossing of the transient spectra does not red-shift significantly with time.

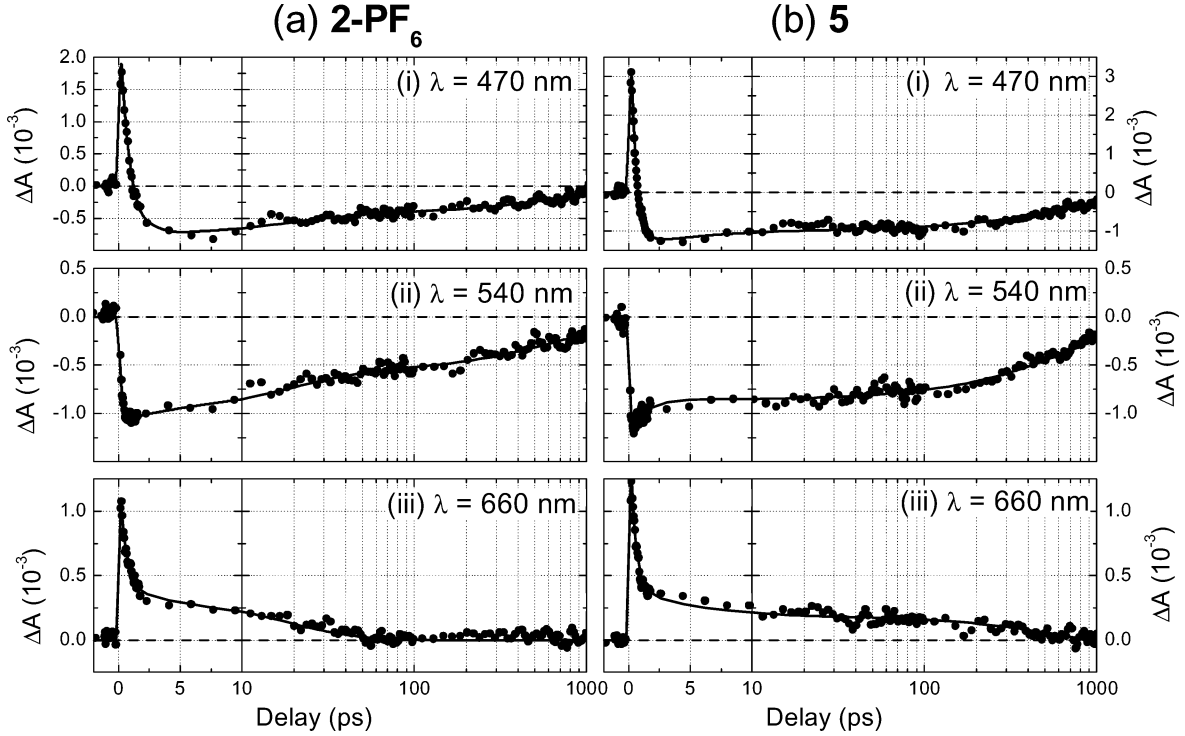

Figure 14. Experimental pump−probe kinetics (points) and multiexponential fits (solid line) for (a) compound **2-PF$_6$** and (b) compound **5** upon 500-nm excitation at selected probe wavelengths: (i) 470 nm, (ii) 540 nm, and (iii) 660 nm.

One possible explanation is that the excitation at 500 nm affects only a spectroscopically distinct portion of the ground-state molecules; i.e., hole burning of the ground-state absorption because of an inhomogeneous broadening of the ensemble.[59] However, given that no red-shifting of the bleach band is observed over the full delay range, this would imply a characteristic time scale for the broadening mechanism of $\tau \gg 1$ ns. Although one could consider this for the case of compound **2-PF$_6$**, where rotation about the B−C bonds between the donor and the acceptor might occur on such a time scale, this is unlikely to be the case for compound **5**, where the −O− bridge should enforce a much more rapid fluctuation in the relative conformation of donor and acceptor.

Thus, to explain the reduced width of the bleach band, we are led to conclude that there are actually two distinct ESA bands in the transient spectra of Figure 13: one band (ESA-I) that is dominant in the wavelength range of ∼550−650 nm and suppresses the bleach band in this region, and a second band (ESA-II) that dominates the signal in the wavelength range of >650 nm.

Concerning the origin of these ESA bands, it is interesting to consider certain features of the differential absorption spectra of compound **2-PF$_6$** upon oxidation and reduction (Figure 13d; refer to Figure 12 for the full spectral range). We note that, upon electrochemical oxidation of compound **2-PF$_6$**, one also does not observe a negative differential absorption of the same shape as the ground-state absorption, mostly due to the fact that a new absorptive feature (labeled band C in Figure 12a) appears, which has a differential peak at 637 nm. Thus, we propose that the same transition is present in the transient spectra of Figure 13, which we identify as the ESA-I band. Based on the assumption that a predominantly HOMO[−2] orbital is involved in the CT transition, this implies that one electron in the higher HOMO[0] orbital relaxes rapidly into the HOMO[−2] vacancy, allowing the transition that corresponds to band C (which corresponds to a vacancy in the HOMO[0] orbital) to be active. The fact that the combined signal of the bleach and ESA-I band does not change shape over the excited-state lifetime implies that the ESA-I band decays with the same kinetics as the recovery of the ground state. This is consistent with the assertion that the transition is between electrons localized on the Fc unit.

Moreover, for the origin of the ESA-II band, we note that, upon reduction of the B-Bipy acceptors, a new absorption band appears in the Vis−NIR region. Hence, we assign the presence of the ESA-II band to the occupation of an initial excited state of similar electronic character to that of the reduced species, which is consistent with the assertion that the orbitals occupied by the excited electron are mostly localized on the B-bipy unit, as suggested by the calculated molecular orbitals. In reference to the comment near the end of the last section, the absence of the absorptive feature in the range of ∼450−500 nm that is observed upon reduction (band F in Figure 12b) is not surprising, given that, in the excited state, the Fc unit is formally oxidized and, hence, becomes more electron-withdrawing, such that this band would be blue-shifted to the short-wavelength edge of the measurement window. Interestingly, one observes some evidence for the onset of another ESA band at this edge in the transient spectra.

To better quantify the relaxation dynamics, in Figure 14, we present the transient absorption kinetics for compounds **2-PF$_6$** (Figure 14a) and **5** (Figure 14b) at three characteristic probe wavelengths: (i) $\lambda_{probe} = 470$ nm (at the high-energy tail of the bleach band), (ii) $\lambda_{probe} = 540$ nm (on the low-energy side of the bleach band), and (iii) $\lambda_{probe} = 660$ nm (ESA-II band). For both compounds, the kinetics exhibit three distinct time scales (<1 ps, ∼5−20 ps, and ∼800 ps), although the relative weights of these components are dependent on the probe wavelength. We fit the positive delay data using a multiexponential fitting function,

$$\Delta A(t) = \sum_{j=1}^{3} A_j \exp\left(-\frac{t}{\tau_j}\right)$$

with global values for the two longer time constants τ_2 and τ_3,

TABLE 2: Parameters from the Multiexponential Fits of the Transient Absorption Kinetics of Compounds 2-PF_6 and 5 (Shown in Figure 14) and Compound 6 (Shown in Figure 15)[a]

compound	τ_1 (ps)	A_1[b]	τ_2 (ps)	A_2	τ_3 (ps)	A_3
			$\lambda_{probe} = 470$ nm			
2-PF_6	0.80 (0.03)	+4.4	**17.8 (1.3)**	−0.46	**810 (33)**	−0.54
5	0.46 (0.02)	+5.1	**4.6 (1.3)**	−0.31	**774 (19)**	−0.69
			$\lambda_{probe} = 540$ nm			
2-PF_6			**17.8 (1.3)**	−0.45	**810 (33)**	−0.55
5	1.13 (0.25)	−0.47			**774 (19)**	−1
			$\lambda_{probe} = 660$ nm			
2-PF_6	0.56 (0.07)	+2.5	**17.8 (1.3)**	+1		
5	0.41 (0.06)	+2.9	**4.6 (1.3)**	+0.45	**774 (19)**	+0.55
6	0.61 (0.04)	+3.3	31.2 (2.4)	+1		

[a] Standard errors given in parentheses. Subscripts denote the time scale in increasing order. Missing values indicate that the additional component did not assist significantly in the fitting of the data. [b] All amplitudes are normalized by $|A_2| + |A_3|$.

the results of which are listed in Table 2. To assess the relative weight of each signal component, the amplitudes in Table 2 are normalized by the combined amplitude of the two slower components, i.e., $A_j \rightarrow A_j/(|A_2| + |A_3|)$.

The kinetics for $\lambda_{probe} = 540$ nm represent the ground-state recovery of the excited ensemble, which, in both compounds, is essentially complete after 1 ns. For compound **2-PF_6**, the fit required an almost 1:1 (0.45:0.55) combination of both a relatively fast picosecond component and a nanosecond component ($\tau_2 = 17.8$ ps, $\tau_3 = 810$ ps), whereas for compound **5**, the ground-state recovery is essentially monoexponential ($\tau_3 = 774$ ps), with the inclusion of a small additional femtosecond decay component ($\tau_1 = 1.3$ ps).

In contrast to the 540-nm data, this femtosecond component is present as a relatively larger and positive absorption signal for both compounds and both $\lambda_{probe} = 470$ nm and $\lambda_{probe} = 660$ nm, with time constants in the range of 0.4−1.1 ps. From control measurements of pure solvents, it is unlikely that these femtosecond transients occur because of pure solvent artifacts, especially given the fact that they are of almost-negligible amplitude specifically in the region of the bleach band ($\lambda_{probe} = 540$ nm). Instead, we attribute these transients to ultrafast intramolecular rearrangement and solvation of the initial excited state, which are typically observed on this time scale.[60,61]

For $\lambda_{probe} = 470$ nm, after the initial femtosecond-induced absorption, the kinetics for compound **2-PF_6** are similar to that of the 540-nm curve, with very similar relative weights for the τ_2 and τ_3 components (0.46:0.54) as for the 540-nm kinetics. The data for compound **5** at 470 nm are also similar to those obtained at 540 nm, except that an additional picosecond transient ($\tau_2 = 4.6$ ps) is present, which indicates the onset of other spectral features at the blue edge of the bleach band. Most striking of all is the comparison of the ESA-II signals ($\lambda_{probe} = 660$ nm) between the two compounds. In the case of compound **2-PF_6**, no signal component on the 810-ps ground-state recovery time scale is observed, and the signal decays completely with the 17.8-ps time constant. In contrast, a majority (0.55) of the ESA-II signal for compound **5** persists on the longer 774-ps time scale. These differences in the decay of the ESA-II signal and the ground-state recovery for both compounds implies the involvement of at least one intermediate electronic state in the relaxation pathway of both compounds (which is essentially "dark" in the probe wavelength range used here), or at least a shift of the reaction coordinates of the excited state away from the Franck−Condon region, where the ESA-II transition is allowed.

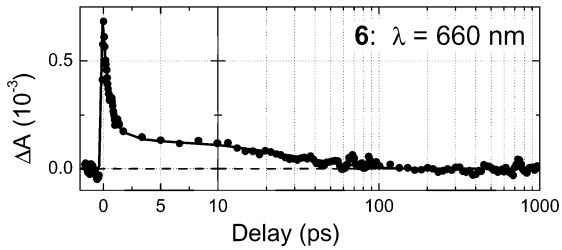

Figure 15. Transient absorption kinetics for $\lambda = 660$ nm (ESA) for compound **6**, with multiexponential fit (solid line).

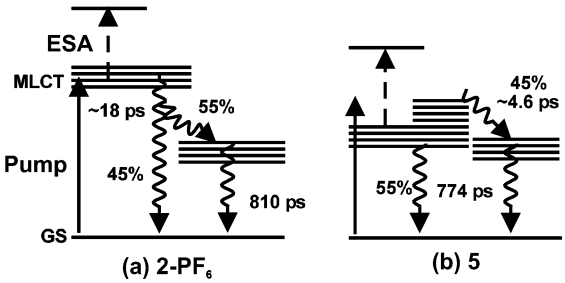

Figure 16. Simplified Jablonksi diagrams for the relaxation of the MLCT states for (a) compound **2-PF_6** and (b) compound **5**.

To understand the factors leading to these differences, we also measured the kinetics for compound **6** for $\lambda_{probe} = 660$ nm, which is displayed in Figure 15 (with the multiexponential fit data included in Table 2). As is evident, the decay of the ESA-II signal for compound **6** is very similar to that of compound **2-PF_6** (and not **5**), in that after an initial femtosecond relaxation, the ESA-II signal decays completely with a time constant of $\tau_2 = 31.2$ ps, albeit some ~10 ps slower than that observed for compound **2-PF_6**. As mentioned previously, the inclusion of compound **6** in the comparison allows one to distinguish characteristic effects that result from the −O− bridge at boron from the structural rigidity of the compounds. Given that the initial excited state is vacated on the same time scale in compounds **2-PF_6** and **6**, this leads us to conclude that this relaxation mechanism relies more on the structural flexibility of the bridging bonds between the donor and the acceptor, which permits the excited state to reach a conformation where either an internal conversion is allowed (possibly involving a through-space bET) or where the Franck−Condon factor for the ESA-II transition becomes negligible. The fact that there is a significant component (0.45) in the ground-state recovery for compound **2-PF_6** on the same 17.8-ps time scale as the decay of the ESA-II signal implies that this portion of the excited molecules decays directly back to the ground state. The remaining fraction of the ensemble branches into an intermediate state with the far-slower (810-ps) ground-state recovery, presumably because of the involvement of additional active modes. These conclusions are summarized in the simplified energy diagram in Figure 16a.

For the case of compound **5**, the appreciable component of decay in the 470-nm and 660-nm kinetics at 4.6 ps, which is absent in the 540-nm data (which has a monoexponential decay of 774 ps), implies that the ground-state recovery of compound **5** from the initial excited and intermediate states proceeds via a similar pathway. However, if this 4.6-ps relaxation mechanism was available to the entire excited ensemble, one would observe a complete decay of the ESA-II signal on the same time scale. We rationalize this by proposing that this fast relaxation pathway is only energetically available to a fraction of the compounds that have sufficient net excess energy to overcome a barrier between the initial excited and intermediate state (Figure 16b),

possibly because of the relatively large bandwidth of the excitation pulse.

Conclusion

We have provided an experimental basis to confirm and better understand the origin of metal-to-ligand charge transfer (MLCT) transitions between donor and acceptor groups that incorporate B−N architecture. A comparison of the UV−Vis spectra for various derivatives and theoretical calculation provides strong evidence that the visible absorption band of the ferrocene−bipyridylboronium (Fc−B-Bipy) compounds studied here result from a direct MLCT transition from Fc-centered orbitals into those of the B-Bipy unit. The electrochemistry data show that the redox properties of the donor and the acceptor are only moderately perturbed from those of the isolated compounds, which is consistent with the localized nature of the theoretically calculated molecular orbitals, while the reduction potential of the acceptor has been shown to correlate with the MLCT transition energy. The correspondence between the UV−Vis spectra upon oxidation/reduction with the excited-state transient absorption spectra also reflect that the initial excited state is qualitatively similar to a superposition of an oxidized-donor and a reduced-acceptor. Of key interest is the effect of structural rigidity in the bridging bonds between the donor and the acceptor, which has been demonstrated to effect the rate and mechanism of the back-electron transfer (bET) strongly. In the case where the acceptor group is free to rotate, relative to the donor (e.g., compound **2**), the initially excited state decays on an ∼18-ps time scale, with a significant portion of the ensemble returning directly to the ground state. In the case where this degree of freedom is hindered (compound **5**), the entire ground-state recovery occurs on an ∼800 ps time scale.

These results will greatly facilitate the rational design of macromolecular assemblies that use these building blocks to achieve efficient charge transfer for applications such as charge injectors for molecular electronics and nonlinear optics. The potential for reversible switching between multiple stable redox states, where the MLCT transition can be present or suppressed, allows the possibility for external electronic control of the linear and nonlinear optical properties of these compounds. The important role of structural factors that affect the bET mechanisms motivates the design of more-rigid systems, to enhance the excited-state lifetime and allow for improved performance in applications based on optically induced charge injection and molecular-based memory storage.

Acknowledgment. The authors gratefully acknowledge funding of this research program by the Deutsche Forschungsgemeinschaft via Forschergruppe 412, "Spin-und Ladungskorrelationen in Niedrigdimensionalen Metallorganischen Festkörpern. P. Z. acknowledges the financial support of the University of Siena (PAR 2003).

References and Notes

(1) Huppman, P.; Arlt, T.; Penzkofer, H.; Schmidt, S.; Bibikova, M.; Dohse, B.; Oesterhelt, D.; Wachtveitl, J.; Zinth, Z. *Biophys. J.* **2002**, *82*, 3186.

(2) Book, L.; Ostafin, A.; Ponomarenko, N.; Norris, J.; Sherer, N. *J. Phys. Chem. A* **2000**, *104*, 8295.

(3) Walker, G.; Maiti, S.; Cowen, B.; Moser, C.; Dutton, P.; Hochstrasser, R. *J. Phys. Chem.* **1994**, *98*, 5778.

(4) Shaheen, S.; Brabec, C.; Sariciftci, N.; Padinger, F.; Fromherz, T.; Hummelen, J. *Appl. Phys. Lett.* **2001**, *78*, 841.

(5) Parisi, J.; Dyakonov, V.; Pientka, M.; Riedel, I.; Deibel, C.; Brabec, C.; Sariciftci, N.; Hummelen, J. *Z. Naturforsch. A: Phys. Sci.* **2002**, *57a*, 995.

(6) Tan, L.; Curtis, M.; Francis, A. *Macromolecules* **2002**, *35*, 4628.

(7) Samok, M.; Williams, D. *J. Chem. Phys.* **1983**, *78*, 1924.

(8) Barlow, S.; Bunting, H.; Ringham, C.; Green, J.; Bublitz, G.; Boxer, S.; Perry, J.; Marder, S. *J. Am. Chem. Soc.* **1999**, *121*, 3715.

(9) Togni, A., Hayashi, T., Eds. *Ferrocenes*; VCH Verlagsgesellschaft: Weinheim, Germany, 1995.

(10) Yang, E.; Chan, M.; Wahl, A. *J. Phys. Chem.* **1980**, *84*, 3094.

(11) Thiel, W.; Priermeier, T.; Fiedler, D.; Bond, A.; Mattner, M. *J. Organomet. Chem.* **1996**, *514*, 137.

(12) Calabrese, J.; Cheng, L.; Green, J.; Marder, S.; Tam, W. *J. Am. Chem. Soc.* **1991**, *113*, 7227.

(13) Alain, V.; Fort, A.; Barzoukas, M.; Chen, C.; Blanchard-Desce, M.; Marder, S.; Perry, J. *Inorg. Chim. Acta* **1996**, *242*, 43.

(14) Pal, S.; Krishnan, A.; Das, P.; Samuelson, A. *J. Organomet. Chem.* **2000**, *604*, 248.

(15) Krishnan, A.; Pal, S.; Nandakumar, P.; Samuelson, A.; Das, P. *Chem. Phys.* **2001**, *265*, 313.

(16) Gilch, P.; Pöllinger-Dammer, F.; Musewald, C.; Michel-Beyerle, M.; Steiner, U. *Science* **1998**, *281*, 982.

(17) Baigar, E.; Gilch, P.; Zinth, W.; Stöckl, M.; Härter, P.; von Feilitzsch, T.; Michel-Beyerle, M. *Chem. Phys. Lett.* **2002**, *352*, 176.

(18) Ruthkosky, M.; Kelly, C.; Zaros, M.; Meyer, G. *J. Am. Chem. Soc.* **1997**, *119*, 12004.

(19) Abbott, L.; Arnold, C.; Ye, T.; Gordon, K.; Perutz, R.; Hester, R.; Moore, J. *J. Phys. Chem. A* **1998**, *102*, 1252.

(20) Damrauer, N.; McCusker, J. *J. Phys. Chem. A* **1999**, *103*, 8440.

(21) Yeh, A.; Shank, C.; McCusker, J. *Science* **2000**, *289*, 935.

(22) Tyson, D.; Luman, C.; Zhou, X.; Castellano, F. *Inorg. Chem.* **2001**, *40*, 4063.

(23) Fabrizi de Biani, F.; Gmeinwieser, T.; Herdtweck, E.; Jäkle, F.; Laschi, F.; Wagner, M. *Organometallics* **1997**, *16*, 4776.

(24) Ding, L.; Ma, K.; Fabrizi de Biani, F.; Bolte, M.; Zanello, P.; Wagner, M. *Organometallics* **2001**, *20*, 1041.

(25) Ma, K.; Fabrizi de Biani, F.; Bolte, M.; Zanello, P.; Wagner, M. *Organometallics* **2002**, *21*, 3979.

(26) Jäkle, F.; Mattner, M.; Preiermeier, T.; Wagner, M. *J. Organomet. Chem.* **1995**, *502*, 123.

(27) Herdtwerk, E.; Jäkle, F.; Opromolla, G.; Spiegler, M.; Wagner, M.; Zanello, P. *Organometallics* **1996**, *15*, 5524.

(28) Jäkle, F.; Priermeier, T.; Wagner, M. *Chem. Ber.* **1995**, *128*, 1163.

(29) Fabrizi de Biani, F.; Jäkle, F.; Spiegler, M.; Wagner, M.; Zanello, P. *Inorg. Chem.* **1997**, *36*, 2103.

(30) Thomson, M.; Roskos, H.; Wagner, M. *Appl. Phys. A* **2004**, *78*, 477.

(31) Hirao, H.; Fujimoto, H. *J. Phys. Chem. A* **2000**, *104*, 6649.

(32) Fiacco, D.; Leopold, K. *J. Phys. Chem. A* **2003**, *107*, 2808.

(33) Anane, H.; Boutalib, A.; Tomás, F. *J. Phys. Chem. A* **1997**, *101*, 7879.

(34) Anane, H.; Boutalib, A.; Nebot-Gil, I.; Tomás, F. *J. Phys. Chem. A* **1998**, *102*, 7070.

(35) Anane, H.; Boutalib, A.; Nebot-Gil, I.; Tomás, F. *Chem. Phys. Lett.* **1998**, *287*, 575.

(36) $\epsilon(\nu) = \epsilon_{max} \exp[-4 \ln 2(\nu - \nu_0)^2/\Delta\nu_{fwhm}^2$.

(37) Using $f \approx 4.32 \times 10^{-9} \int \epsilon(\nu)\, d\nu$, e.g., the relationship from Klessinger, M.; Michl, J. *Excited States and Photochemistry of Organic Molecules*; VCH Publishers: New York, 1995.

(38) Turro, N. *Modern Molecular Photochemistry*; University Science Books: Mill Valley, CA, 1991.

(39) Birks, J. *Photophysics of Aromatic Molecules*; Wiley: New York, 1970.

(40) Nagasawa, Y.; Passino, S.; Joo, T.; Fleming, G. *J. Chem. Phys.* **1997**, *106*, 4840.

(41) All calculations were performed with Gaussian 98, Revisions A3−A9, Gaussian, Inc., Pittsburgh, PA, 1999.

(42) Becke, A. *J. Chem. Phys.* **1993**, *98*, 5648.

(43) Perdew, J. *Phys. Rev. B* **1986**, *33*, 8822.

(44) Fuentealba, P.; von Szentpaly, L.; Preuss, H.; Stoll, H. *J. Phys. B* **1985**, *18*, 1287.

(45) Using the method described for the isolated ferrocene molecule, we obtained r(CC) = 142.2 pm and r(Fe−C) = 204.9 pm), as compared to the experimentally determined gas-phase values of r(CC) = 143.1 pm and r(Fe−C) = 205.8 pm (from Bohn, R.; Haaland, A. *J. Organomet. Chem.* **1966**, *5*, 470).

(46) Burke. K., Gross, E., Joubert, D., Eds. *Lecture Notes in Physics*; Springer: Heidelberg, 1998; Vol. 500.

(47) Seneviratne, D.; Uddin, J.; Swayambunathan, V.; Schlegel, H.; Endicott, J. *Inorg. Chem.* **2002**, *41*, 1502.

(48) Gilch, P.; Pöllinger-Dammer, F.; Steiner, U.; Michel-Beyerle, M. *Chem. Phys. Lett.* **1997**, *275*, 339.

(49) Daub, J.; Engl, R.; Kurzawa, J.; Miller, S.; Schneider, S.; Stockmann, A.; Wasielewski, M. *J. Phys. Chem. A* **2001**, *105*, 5655.

(50) Zhu, Y.; Wolf, M. *J. Am. Chem. Soc.* **2000**, *122*, 10121.

(51) Malaun, M.; Reeves, Z.; Paul, R.; Jeffery, J.; McCleverty, J.; Ward, M.; Asselberghs, I.; Clays, K.; Persoons, A. *Chem. Commun.* **2001**, 49.

(52) Thander, A.; Mallik, B. *Proc. Indian Acad. Sci. (Chem. Sci.)* **2000**, *112*, 475.
(53) Hünig, S.; Wehner, I. *Heterocycles* **1989**, *28*, 359.
(54) Riedle, E.; Beutter, M.; Lochbrunner, S.; Piel, J.; Schenkl, S.; Spörlein, S.; Zinth, W. *Appl. Phys. B* **2000**, *71*, 457.
(55) Fork, R.; Shank, C.; Hirlimann, C.; Yen, R.; Tomlinson, W. *Opt. Lett.* **1983**, *8*, 1.
(56) Reed, M.; Steiner-Shepard, M.; Armas, M.; Negus, D. *J. Opt. Soc. Am. B* **1995**, *12*, 2229.
(57) Huber, R.; Satzger, H.; Zinth, W.; Wachtveitl, J. *Opt. Commun.* **2001**, *194*, 443.
(58) Ekvall, K.; van der Meulen, P.; Dhollande, C.; Berg, L.; Pommeret, S.; Naskrecki, R.; Mialocq, J. *J. Appl. Phys.* **2000**, *87*, 2340.
(59) Brito Cruz, C.; Fork, R.; Knox, W.; Shank, C. *Chem. Phys. Lett.* **1986**, *132*, 341.
(60) Fleming, G.; Cho, M. *Annu. Rev. Chem.* **1996**, *47*, 109.
(61) Kahlow, M.; Jarzeba, W.; Kang, T.; Barbara, P. *J. Chem. Phys.* **1989**, *90*, 151.